Evolution law of overall damage of concrete gravity dam under near-fault ground motion

Yafei Zhai (yfzhai@hhu.edu.cn)
Hohai University https://orcid.org/0000-0003-2802-3725
Liaojun Zhang
Hohai University https://orcid.org/0000-0003-0894-8034
Hanyun Zhang
Hohai University
Tianxiao Ma
Hohai University
Binghui Cui
Hohai University

Research Article

Keywords: Concrete gravity dams, Near-fault ground motions, Directivity pulse, Fling-step pulse, Dynamic response, Overall damage evolution

Posted Date: April 27th, 2021

DOI: https://doi.org/10.21203/rs.3.rs-463533/v1

Evolution law of overall damage of concrete gravity dam under near-fault ground motion

Yafei Zhai[1], Liaojun Zhang[1,*], Hanyun Zhang[1], Tianxiao Ma[1], Binghui Cui[2]

[1] College of Water Conservancy and Hydropower Engineering, Hohai University,Nanjing, Jiangsu province, 210098, China; yfzhai@hhu.edu.cn; zhanghanyun@hhu.edu.cn; tianxiaoma@hhu.edu.cn
[2] College of Civil and Transportation Engineering, Hohai University,Nanjing, Jiangsu province, 210098, China; bhcui99@hotmail.com
* Correspondence: ljzhang@hhu.edu.cn

Abstract: Strong earthquake cases of concrete gravity dams show that the foundation damage has an important influence on the seismic response and damage characteristics of the dam body. Compared with non-pulse ground motions, pulse-like near-fault ground motions have a wider response spectrum sensitive zone, which will cause more modes of the structure to respond, resulting in more serious damage to the structure. In order to study the real dynamic damage characteristics of concrete gravity dams under the action of near-fault ground motions, this paper takes Koyna gravity dam as the object and establishes a multi-coupling simulation model that can reasonably reflect the dynamic damage evolution process of dam concrete and foundation rock mass. A total of 12 near-fault ground motion records with three types of rupture directivity pulse, fling-step pulse and non-pulse are selected, deep research on the overall damage evolution law of concrete gravity dams. Considering the additional influence of different earthquake mechanisms, different site types and other factors on the study, the selected ground motion records are from the same seismic events (Chi-Chi), the same direction but different stations. The results show that the foundation of the concretes gravity dam often get damaged before the dam body under the action of strong earthquakes. Compared with the near-fault non-pulse ground motion, the structural damage of the gravity dam under the action of the near-fault directivity pulse ground motion is significantly increased, and causes greater damage and displacement response to the dam body. The near-fault fling-step pulse ground motion has the least impact on the dynamic response of the gravity dam structure.

Keywords: Concrete gravity dams; Near-fault ground motions; Directivity pulse; Fling-step pulse; Dynamic response; Overall damage evolution

1. Introduction

Earthquake disaster survey data show that after an earthquake, major damage often occurs in the zone near the epicenter (Eftekhari et al. 2020). Based on this phenomenon, the seismic engineering community and relevant departments have begun to pay great attention to and study the characteristics of near-fault ground motions. However, due to the uncertainty of earthquake occurrence, there are few near-fault ground motion records obtained from actual records. Therefore, the study of near-fault pulse-type ground motions for a long period of time has highlighted the problem of insufficient data. A large number of near-fault seismic data were obtained from several strong earthquakes until the end of the last century, especially the 1994 Northridge earthquake in the United States (Suarez-Villa and Walrod 2010), the Kobe earthquake in Japan in 1995 (Yujia et al. 2013) and the Chi-Chi earthquake in Taiwan in 1999 (Kate et al. 2011). These acquired strong earthquake records provide valuable data for studying near-fault ground motion characteristics. Research on near-fault seismic records shows that the long-period, short-duration and high-speed pulses have a significant impact on the seismic safety of structures (Bhagat et al. 2018; Yang et al. 2019; Li et al. 2020). In China, the construction of high dams and large reservoirs is mainly concentrated in the western region, which is rich in hydropower resources, but faces the inevitable seismic safety problem. Therefore, a correct understanding of the impact of near-fault ground motions on the nonlinear dynamic damage and failure of gravity dams is of great significance to comprehensively and accurately assessing the seismic resistance of large dam projects.

Strong earthquakes may cause damage and cracking of the concrete dam, threatening the safety of the dam. In the seismic design and research of high concrete dams, we should break through some traditional concepts and methods that are difficult to reflect reality. For example, in the seismic analysis of traditional high concrete dams, the foundation rock mass is mostly used as linear elastic materials or DP elastoplastic models are used (Ansari et al. 2016; Sadeghi et al. 2020; Li et al. 2021). But the simulation cannot accurately reflect the nonlinear performance and stress redistribution phenomenon of rock when subjected to external loads that exceed their tensile and compressive strength (Guo et al. 2020; Zhang et al. 2021). In fact, the damage and failure of the dam foundation rock mass is also an important part of the overall seismic design and analysis in a gravity dam. Generally in the dam foundation rock mass, there are a large number of micro-cracks and micro-cracks, resulting in the low tensile properties of the dam foundation material. Under

the reciprocating action of earthquakes, the dam foundation rock mass often cracks and fails first, which releases seismic energy to a certain extent, thereby reducing the stress concentration of the dam heel and preventing the dam from cracking and damage. And the measured data of the gravity dam subjected to the earthquake also confirms this (after the earthquake, the Koyna gravity dam foundation interface was drilled and sampled, and it was found that the concrete and the bedrock cemented well, and no signs of cracking at the dam foundation interface were found, and the leakage of the dam foundation did not change significantly after the earthquake) (Chen et al. 2014). The damage analysis of the foundation rock mass is an important part of the damage analysis of multi-coupling system of high concrete dam. However, in the current research on the damage of the high concrete dam system, the damage of the dam body is mostly studied, and the results of the overall damage of the dam foundation are few. In order to truly understand the seismic performance of the concrete gravity dam structure, it is necessary to conduct an in-depth study on the overall dynamic damage evolution process of the dam foundation.

With people's understanding of near-fault ground motions, scholars have studied the damage effects of dams under near-fault ground motions (Hadiani. 2013; Wang et al. 2014; Zou et al. 2017). Bayraktar A et al. (2010) discussed the dynamic response of the reservoir zone to the gravity dam under the action of a near-fault pulse earthquake, and studied the nonlinear dynamic response of the dam-reservoir-foundation system under the action of near-fault ground motions. Akkose M et al. (2010) etc Studied the nonlinear dynamic response of the dam-reservoir-sediment-foundation system to near-fault ground motions and far-fault ground motions, revealing the change law of dam crest displacement and plastic deformation caused by near-fault ground motions; Wang Gaohui et al. (2014) conducted a comparative analysis of the effects of near-fault directivity pulse and far-fault ground motions on the cumulative damage characteristics of concrete gravity dams; Huang J (2015) studied the influence of the spatial variability of near-site vibration on the cumulative damage effect of gravity dams; Yazdani Y et al. (2017) studied the nonlinear seismic response of gravity dams under the action of near-fault ground motions and equivalent pulses; Gorai S et al. (2021) studied the seismic behavior of aged concrete gravity dams to near source and far source ground motions. However, the above research only considers the damage distribution of the dam body, ignoring the damage and failure of the foundation rock mass under the action of the earthquake. In addition, there is still a lack of research on the dynamic damage of the concrete gravity dam under the action of different types of near-fault ground motions. Taking the Koyna concrete gravity dam as an example, based on the finite element software ABAQUS, a multi-coupling simulation model that can reasonably reflect the dynamic damage evolution process of dam concrete and dam foundation rock mass is established. From the Chi-Chi earthquake (Kao 2002), a total of 12 near-fault ground motions with directional pulses, fling-step pulse and non-pulse are selected as input, and the cumulative damage and energy characteristics of the Koyna concrete gravity dam under near-fault earthquakes are analyzed. This research reveals the evolution of the overall damage of concrete gravity dams under different types of near-fault ground motions. The research results provide references for the seismic design of concrete gravity dams.

2. Near-fault ground motion characteristics and selection methods

The long-term accumulation of energy in the crustal rock mass causes the rock formation to rupture and form an earthquake. It is generally believed that the near-fault refers to the zone not more than 20 km away from the fracture surface (Bray et al. 2004). Pulse-like near-fault ground motions belong to a type of near-fault ground motions with obvious characteristics and greater destructive power. They can be divided into two types: rupture directivity pulse ground motions and fling-step pulse ground motions. Short duration and large energy input structure are the main characteristics of pulsed ground motions (Durucan et al. 2021). The directional pulse ground motion contains obvious two-way velocity pulses and a larger pulse period (Fig.1), while the fling-step pulse ground motion contain unidirectional velocity and large pulses (Fig. 2).

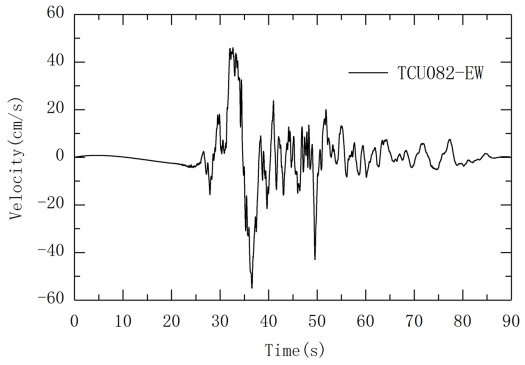

Fig.1 Velocity time history of directivity pulse ground motion

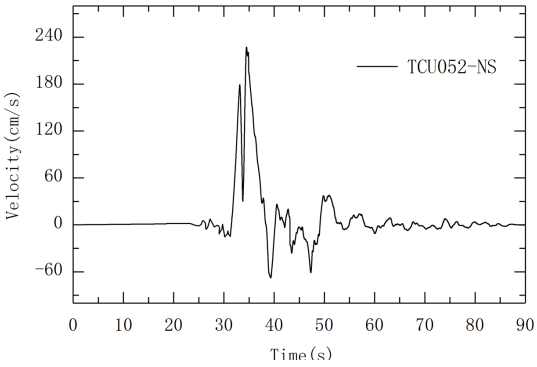

Fig.2 Velocity time history of fling-step pulse ground motion

In this paper, the following selection principles are determined for the ground motion records of the pulse-like near-fault ground motions: the fault distance meets the general definition of near-site vibration principle (distance from the fracture surface is not more than 20 km); PGV/PGA>0.2s. In order to distinguish it from near-fault pulse ground motions, with PGV/PGA<0.2s are defined as non-pulse near-fault ground motions. According to the above-mentioned selection principle and the basic characteristics of directivity pulse and fling-step pulse, 12 ground motions of near-fault directivity pulse, fling-step pulse and non-pulse ground motions are selected respectively. Taking into account the additional influence of different earthquake mechanisms, different site types and other factors on the study, the ground motion records selected in this paper are from the same earthquake (Chi-Chi), seismic wave records of different stations in the same direction. See Table 1 for the characteristics of various types of ground motion parameters. In the Table 1, T_{pv} is the pulse period, $D_{5\text{-}95}$ represents 5%-95% energy duration, and PGA, PGV, and PGD represent peak ground acceleration, velocity and displacement respectively.

Table 1 Near-fault ground motion characteristic parameters

Type of earthquake	No	Station and direction	Fault distance/km	PGA /cms^{-2}	PGV /cms^{-1}	PGD /cm	PGV /PGA	T_{pv}/s	$D_{5\text{-}95}$/s
Directivity pulse	1	TCU050-EW	9.49	143.13	36.83	61.24	0.26	9.56	27.0
	2	TCU051-EW	7.64	157.17	53.85	73.81	0.37	10.38	28.9
	3	TCU056-EW	10.48	153.04	42.21	54.36	0.24	8.85	31.8
	4	TCU082-EW	5.16	221.03	54.93	94.95	0.28	8.10	27.0
Fling-step pulse	5	TCU067-EW	0.66	350.76	151.21	210.37	0.43	11.96	16.7
	7	TCU075-EW	0.89	325.67	109.55	96.51	0.33	4.99	31.2
	8	TCU076-EW	2.74	337.93	69.26	35.23	0.21	4.73	29.5
	8	TCU128-EW	13.13	143.99	60.58	145.39	0.42	9.02	20.6
Non-pulse	9	TCU071-EW	5.80	518.53	52.30	16.08	0.10	-	24.6
	10	TCU072-EW	7.08	467.95	71.93	50.45	0.15	-	24.0
	11	TCU078-EW	8.20	438.81	40.24	30.25	0.09	-	26.1
	12	TCU079-EW	10.97	580.91	70.54	7.54	0.11	-	26.9

In order to avoid the impact of acceleration amplitude, this paper modulates the 12 selected near-fault seismic waves with the acceleration peak value amax=0.2g. Fig.3 shows the average acceleration response spectra of directivity pulse, fling-step pulse and non-pulse near-fault ground motions after amplitude modulation under 5% damping ratio. As shown in the figure, from the peak of the average acceleration response spectrum, the relationship between the three is directivity pulse > non-pulse > fling-step pulse. When the period T < 0.38s, the magnitude order of the average value of the spectral acceleration is non-pulse > directivity pulse > fling-step pulse. When the period T is within the range of 0.38~0.78s, the non-pulse and the directivity pulse ground motion acceleration spectrum increased alternately, and all are greater than the mean value of the fling-step pulse ground motion acceleration spectrum. When the period T ≥ 0.78s, the mean value of the directivity pulse acceleration spectrum is significantly greater than that of the non-pulse. Fig.4 shows the average velocity response spectra of directivity pulse, fling-step pulse and non-pulse ground motions after amplitude modulation. It can be seen from the figure that when the period T is small, the average velocity response spectrum of the near-fault directivity pulse and non-pulse ground motions is greater than that of the fling-step pulse ground motions. For long-period, the relationship between the three is fling-step pulse >

directivity pulse > non-pulse.

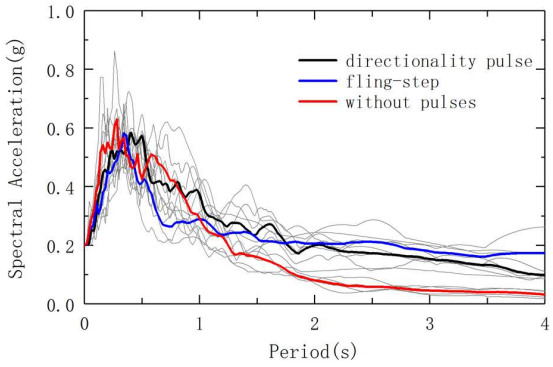

Fig.3 Acceleration response spectrum

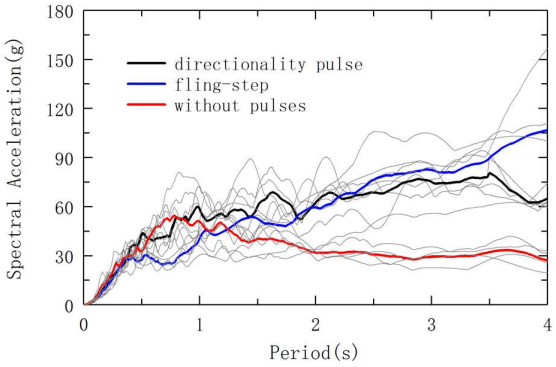

Fig.4 Speed response spectrum

Fig.5 shows a set of acceleration, velocity and displacement time history curves recorded by different types of near-fault ground motions after amplitude modulation. It can be seen from the velocity time history curve that the directivity pulse type ground motion velocity time history curve contains obvious long-period, large-value, and short-duration two-way velocity pulse effects. The fling-step type ground motion contains unidirectional speed big pulse.

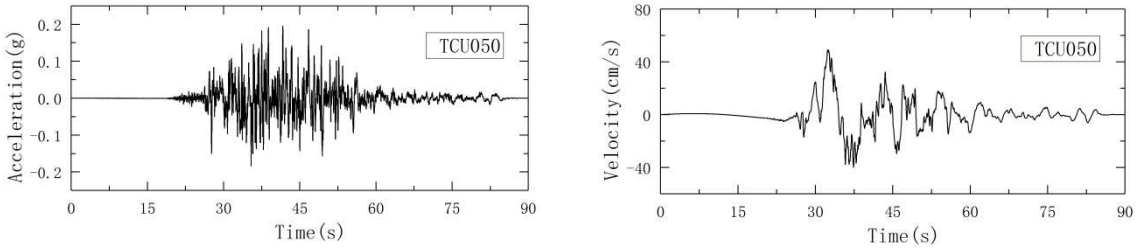

(a) Directivity pulse

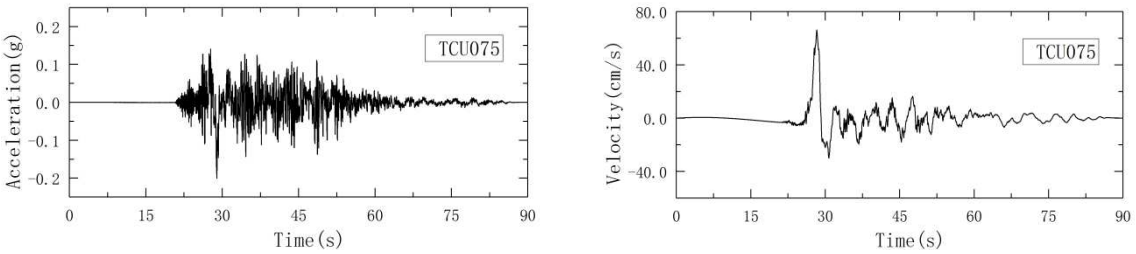

(b) Fling-step pulse

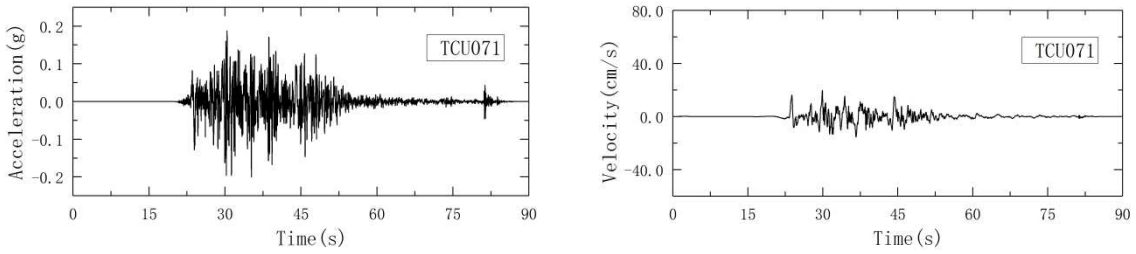

(c) Non-pulse

Fig.5 Curves of acceleration and velocity of the typical near-fault ground motion

3. Concrete plastic damage model

Because concrete is under complex stress state, the evolution law of tensile damage and compression damage is different. Therefore, this paper uses a dual scalar damage model to simulate the dynamic damage and cracking of concrete, and defines two independent damage variables to describe the material. Deterioration of elastic rigidity caused by damage during tension and compression. Fig.6 and Fig.7 show the schematic diagrams of concrete damage under tension and uniaxial compression respectively.

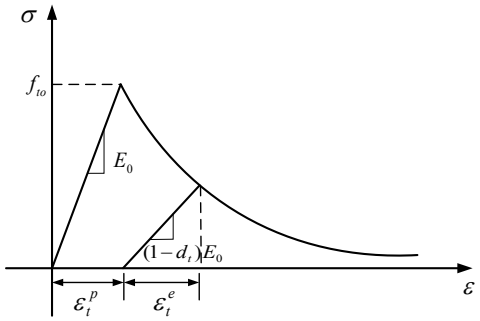

Fig.6 Schematic diagram of concrete uniaxial tensile damage

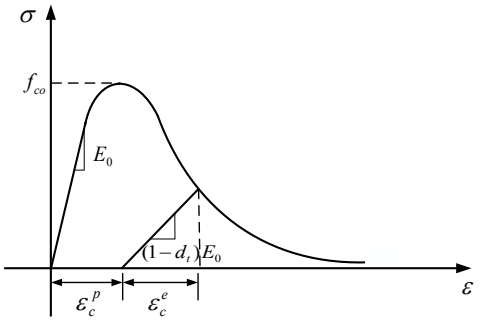

Fig.7 Schematic diagram of concrete uniaxial compression damage

The constitutive relationship of the concrete plastic damage model is as follows:

$$\sigma_t = (1-d_t)E_0(\varepsilon_t - \varepsilon_t^{\,p}) \tag{1}$$

$$\sigma_c = (1-d_c)E_0(\varepsilon_c - \varepsilon_c^{\,p}) \tag{2}$$

In the formula: σ_t and σ_c respectively represent the tensile and compressive stresses of the concrete; d_t and d_c respectively tensile damage factor and compression damage factor; ε_t and ε_c represent tensile and compressive strains respectively; ε_t^p and ε_c^p respectively represent plastic strain in tension and plastic strain in compression; E_0 is the initial elastic modulus.

The model uses the yield function proposed by Lee and Fenves to consider the different strength evolution under tension and compression (Lee et al. 1998). The evolution of yield surface is controlled by variable tensile plastic strain and compressive plastic strain. The yield equation is as follows:

$$F = \frac{1}{1-\alpha}\left(\bar{q} - 3\alpha\bar{p} + \beta(\varepsilon^p)\langle\hat{\sigma}_{\max}\rangle - \gamma\langle-\hat{\sigma}_{\max}\rangle\right) - \bar{\sigma}_c(\varepsilon^p) = 0 \tag{3}$$

$$\beta = \frac{\bar{\sigma}_c(\varepsilon_c^p)}{\bar{\sigma}_t(\varepsilon_t^p)}(1-\alpha) - (1+\alpha) \qquad \bar{p} = -\frac{1}{3}\mathrm{tr}(\bar{\sigma})$$

Where α and γ are size-independent material constants ($0 \le \alpha \le 1$, γ default value is 3), $\bar{\sigma}_c$ and $\bar{\sigma}_t$ are the effective compressive and tensile stress tensors respectively; $\hat{\bar{\sigma}}_{\max}$ is the algebraic maximum eigenvalue (maximum effective stress) of the effective stress tensor $\bar{\sigma}$; $\bar{q}$ is the effective mises equivalent stress.

The flow law of the plastic damage model adopts the non-associated flow law, and its plastic potential function is:

$$G = \sqrt{(\xi\sigma_{t0}\tan\varphi)^2 + \bar{q}^2} - \bar{p}\tan\varphi \tag{4}$$

Where: ξ is the eccentricity of the plastic potential function of concrete; σ_{t0} is the uniaxial stress at failure; φ is the expansion angle of the concrete yield surface during the strengthening process. According to relevant research results, the value of the concrete expansion angle is 36° ~42°.

4. Overall dynamic damage model and verification of gravity dam

In order to truly simulate the impact of ground motion on the damage of the overall system of a concrete gravity dam, unlike the traditional model that considers the foundation as linear elastic or DP plastic, this paper extends the concrete plastic damage model (CDP) to the foundation rock based on the similarity of dam body concrete material and rock materials (Guo et al. 2020). Taking the Koyna concrete gravity dam project as an example, the overall damage mechanics model of the concrete gravity dam body-reservoir water-foundation is established. In order to verify its reliability, the measured seismic waves of Koyna dam is used as input, and the Westergaard method is used to simulate hydrodynamic effects. After considering the dissipated energy of the system to the remote ground (Gao et al. 2021), the seismic response damage analysis of the gravity dam body-reservoir-foundation overall damage force system was carried out, and the analysis results were compared with the actual earthquake damage.

4.1. *Dynamic damage finite element model*

Koyna gravity dam has always been a classic case of concrete dam dynamic analysis. On December 11, 1967,

the Koyna gravity dam in India suffered a magnitude 6.5 earthquake. The depth of the reservoir is 91.75m when the earthquake occurred. The earthquake caused many horizontal cracks on dam body, mainly concentrated near the elevation of 629.0 m (as shown in Fig.8). This paper takes the Koyna gravity dam as the research object and selects a typical retaining dam section of the dam for analysis. The upper, downstream and depth directions of the foundation range are each twice the dam height. The dam body-reservoir-foundation coupling model is shown in Fig.9.

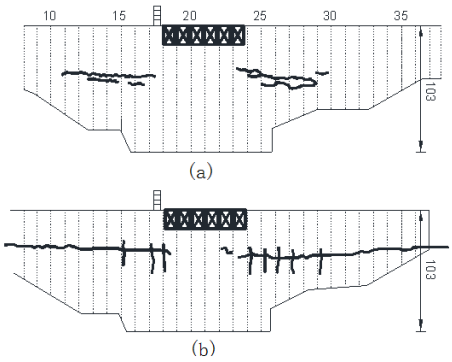

Fig.8 Earthquake damage to Koyna Dam (a: upstream view, b: downstream view)

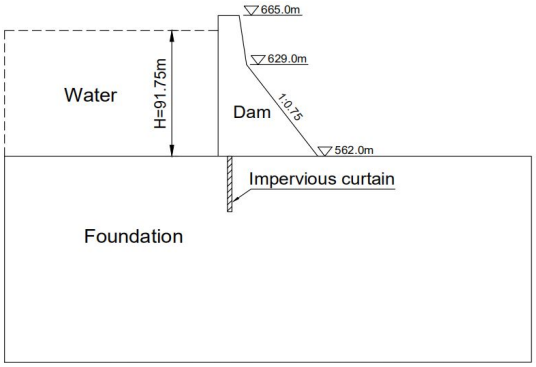

Fig.9 Dam body-reservoir water-foundation model

Considering the effects of vertical and horizontal seismic waves at the same time, the seismic wave is based on the measured seismic records of Koyna dam in 1976. The peak acceleration of the horizontal seismic wave is 0.474g (Fig.10), and the peak acceleration of the vertical seismic wave is 0.312g (Fig.11). Adopt viscoelastic artificial boundary to consider the influence of ground radiation damping. The dam concrete material parameters used in the calculation are: dynamic elastic modulus 31 GPa, density 2643 kg/m^3, Poisson ratio is 0.15, fracture energy 200 N/m, dynamic tensile strength 2.9 MPa. Base rock material parameters: elastic modulus 20 GPa, density 2700 kg/m^3, Poisson ratio is 0.20, cohesive force 2.0 MPa, friction coefficient 1.16, base on moercoulomb criterion inferred the tensile strength of the bedrock material to be 1.28 MPa (Chen et al. 2014). The initial in-situ stress field is in accordance with the requirements of the engineering rock mass classification standard regarding the initial stress field evaluation. The vertical in-situ stress is the weight of the rock mass γh, and the horizontal in-situ stress is taken as 1.2 γh. Considers that the damping force changes with the opening and closing of the crack, and the Rayleigh damping coefficient is taken as = 0 and = 0.0032.

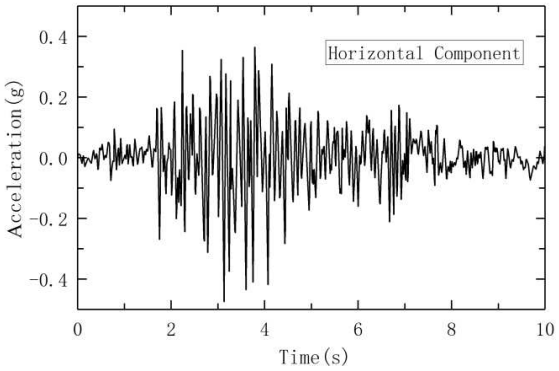

Fig.10 Acceleration time history curve of horizontal seismic wave

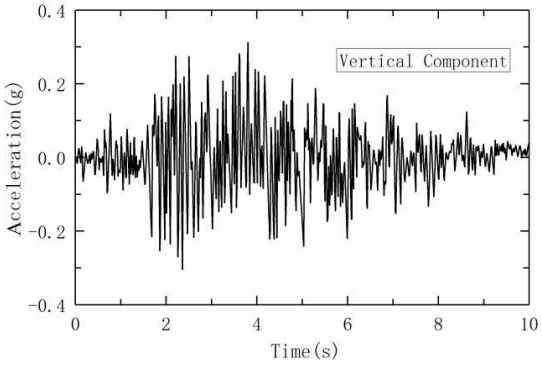

Fig.11 Acceleration time history curve of vertical seismic wave

4.2. *Damage evolution characteristics of Koyna gravity dam*

Under the action of earthquake, the overall damage zone of the gravity dam at different times is shown in Fig.12. After considering the nonlinear damage of the dam body and the foundation, due to the low tensile strength of the dam foundation rock mass, at t=1.92 s, the dam foundation rock mass firstly began to have damage cracks (Fig.12(a)). With the increasing of the duration of ground motion, the damage zone of the bedrock expands about 23.1m in the depth direction, and then begins to expand obliquely downstream. At t =3.64 s, damage cracks began to appear in the dam body, at this time, the depth of the damage cracks in the bedrock is about 34.3 m (Fig.12(b)); After the ground motion is over, the final damage zone of the dam system is shown in Fig.12(d). Dam body damage is mainly concentrated near the elevation of the downstream

break slope. The damage of the dam foundation mainly occurred in the bedrock at the heel of the dam, and it extended about 35.2 m in the depth direction, but the impervious curtain was not damaged. It can be seen that after considering the damage of the dam foundation, the foundation part of the concrete gravity dam will be damaged before the dam body under the action of the earthquake. It shows that it is necessary to consider the overall plastic damage of the dam body and the bedrock in the seismic analysis of the concrete gravity dam.

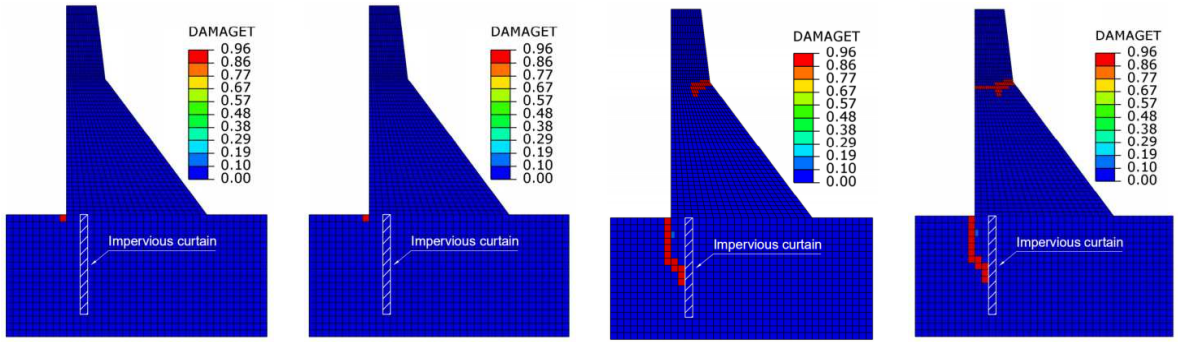

(a) t=1.92s (b) t=3.64s (c) t=4.26s (d) t=10s

Fig.12 Damage zone of gravity dam at different times

Unlike only considering the dam body concrete as the plastic damage model, after considering the plastic damage of the foundation, the concrete at the heel of the dam did not produce cracking damage, and the anti-seepage curtain did not damage. This is because after considering the nonlinear damage of the foundation rock mass, under the action of an earthquake, damage cracks appear in the foundation rock at the dam heel, which releases the stress on the dam body, thereby avoiding the damage and failure of the concrete at the dam heel. This also shows that only the dam body is considered as a plastic damage model, and the bedrock is considered as a linear elastic or elastoplastic model, which cannot accurately simulate the damage evolution process of a concrete gravity dam multi-coupling system under seismic response. The actual survey after the earthquake also showed that the cracks of the Koyna gravity dam caused by the earthquake were mainly concentrated near the elevation of 629.0 m (Fig.8). Core-drilling sampling at the interface of the dam foundation found that the concrete and bedrock cemented well, no signs of cracking at the interface of the dam foundation were found, and there was no significant change in the leakage of the dam foundation after the earthquake. The simulation results in this paper are in good agreement with the actual earthquake damage.

5. Dynamic response and damage characteristics of gravity dams under near-fault ground motions

In order to study the influence of near-fault ground motions on the dynamic damage of the overall system of concrete gravity dams, this paper uses the different types of near-fault ground motion records selected in section 2 to modulate the amplitude of the acceleration peak amax=0.2g as the ground motion input (only consider ground motion horizontal component). The effects of three types of near-fault ground motions on the overall damage evolution of the concrete gravity dam foundation are studied from the aspects of plastic damage zone, dissipated energy and displacement response of the dam.

5.1. *Evolution law of overall damage of dam body and foundation*

Under the action of near-fault ground motions, the damage and failure process of gravity dam body and foundation material is the deterioration of the mechanical properties of the material caused by the growth, expansion and connection of micro-cracks inside it. It is also an irreversible and energy-consuming evolution process of the internal structure of the material. Fig.13 shows the overall damage distribution of gravity dams under different types of near-fault ground motions. The blue zone indicates that the material is not damaged, and the red zone indicates that the material is damaged by tensile damage. It can be seen from the figure that under the action of the three types of near-fault ground motions, the dam foundation rock mass materials have suffered serious tensile damage. It shows that under the action of earthquake, the dam foundation rock mass is the weak link of the earthquake resistance of the concrete gravity dam. It is necessary to pay more attention to the earthquake resistance analysis of the concrete gravity dam. When the near-fault directivity pulse ground motion is used as input, the overall damage of the gravity dam foundation is shown in Fig.13(a). Both the concrete material of the dam body and the rock material of the foundation suffered serious damage and failure.

Among them, the damage of the dam foundation mainly occurred in the bedrock part at the heel of the dam and extended along the depth direction. The concrete damage of the dam body is concentrated in the downstream break slope and spreads upstream. Under the action of the near-fault fling-step pulse ground motion, the overall damage of the gravity dam is shown in Fig.13 (b). It can be seen that there is no damage to the dam body of the concrete gravity dam. Similarly, the damage of the dam foundation mainly occurs in the bedrock part at the heel of the dam and extends in the depth direction. Under near-fault non-pulse ground motions, as shown in Fig.13 (c), similar to the directivity pulse and fling-step pulse ground motions, the dam foundation damage occurs in the bedrock part at the dam heel and extends along the depth direction. Compared with the near-fault directivity pulse ground motion, the dam concrete material is less damaged.

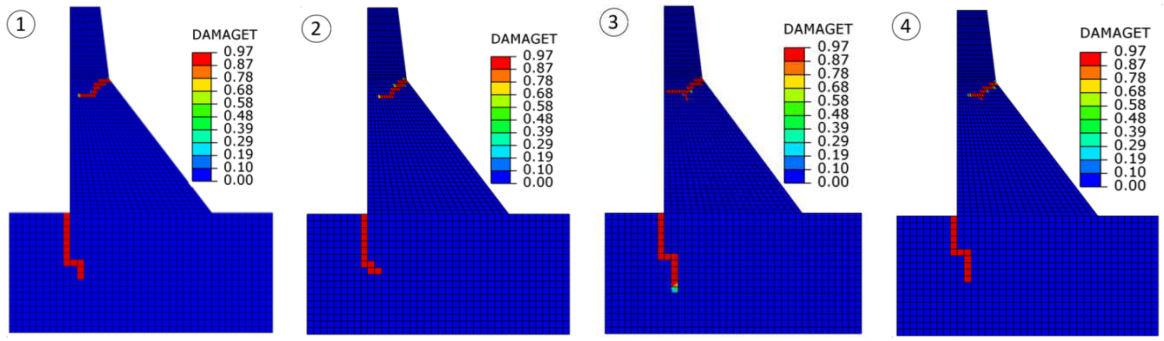

(a) Directivity pulse

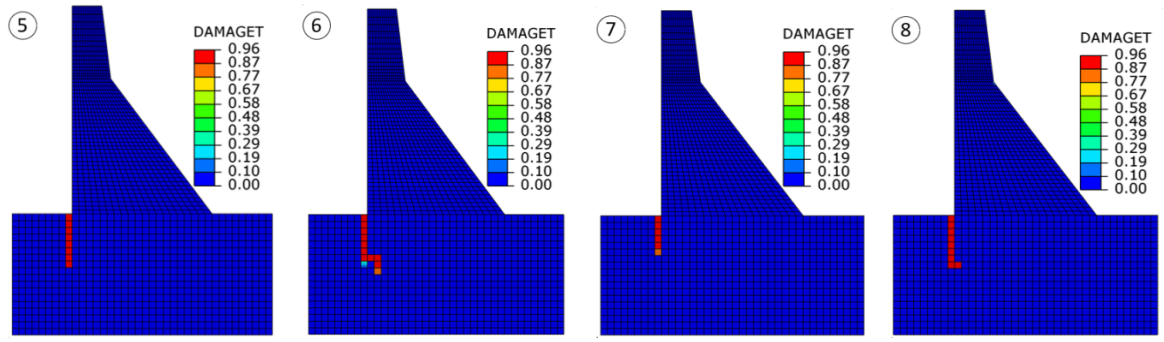

(b) Fling-step pulse

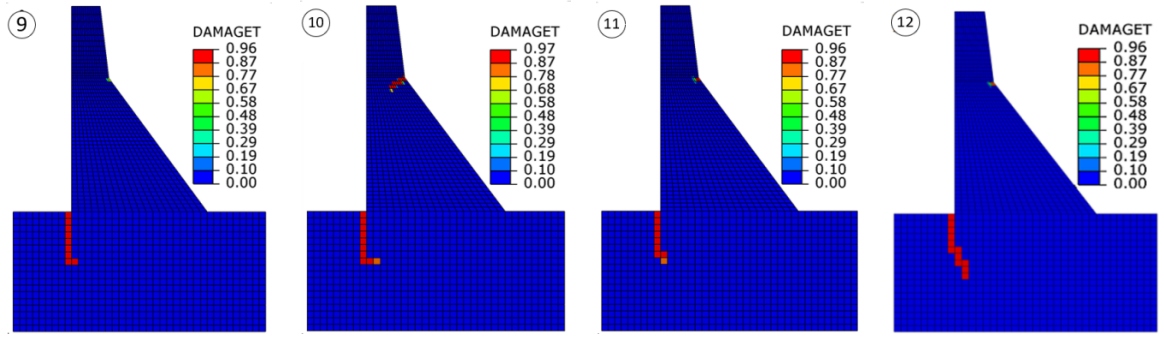

(c) Non-pulse

Fig.13 Dam damage zone of near-fault ground motions (1,2...represent the seismic wave number)

The paper defines that there are damage cracks when the damage factor D=0.75. Table 2 shows the characteristic values of the crack length of the concrete gravity dam under the action of three types of near-fault ground motions. From the perspective of the development of damage and cracks in the dam body, Under the action of near-fault directional pulse ground motions, the average damage crack length at the downstream bend of the dam body is 19.6m. Fling-step pulse ground motion did not cause damage to the concrete of the dam. Under the action of non-pulse ground motions, the average damage crack length at the downstream break of the dam body is 3.9m. From the perspective of the development of dam foundation damage and cracks, under the action of three types of near-fault ground motions, the average crack length at

the base rock of the dam heel is 38.1, 26.5 and 31.2m, respectively. In summary, from the perspective of the damage zone of the concrete gravity dam, under three types of near-fault ground motions, the near-fault directivity pulse ground motion has the greatest impact on the damage and failure of the concrete gravity dam, and the near-fault non-pulse ground motion is the second place, the near-fault fling-step pulse ground motion has the least impact on the damage and failure of the concrete gravity dam.

Table 2 Crack length of the gravity dam under near-fault ground motions (m)

Type of earthquake	Directivity pulse				Fling-step pulse				Non-pulse			
No	1	2	3	4	5	6	7	8	9	10	11	12
Dam body crack length	20.5	18.9	22.5	16.8	-	-	-	-	1.0	10.6	2.1	1.8
Average value	19.6				-				3.9			
Dam foundation crack length	38.4	34.7	41.3	37.9	25.2	32.8	20.0	28.1	28.1	31.4	27.1	38.0
Average value	38.1				26.5				31.2			

5.2. *dissipated energy characteristics of dam body and foundation*

The damage and failure of the gravity dam will accumulate in the form of dissipated energy under the action of an earthquake (Zhang et al. 2013; Wang et al. 2015; Zhai et al. 2020) . Therefore, understanding the dissipated energy characteristics of gravity dam structures under earthquake action is of great significance to understanding the damage and failure process. This paper is based on the CPD model, while considering the damage and failure of the dam body and bedrock, the gravity dam is analyzed for nonlinear seismic response, and the dissipated energy of the dam under different types of near-fault ground motions is analyzed and compared. The CDP model used in this paper can consider both plastic dissipated energy and damage dissipated energy. The specific calculation formulas for damage dissipated energy M_D and plastic dissipated energy M_P are

$$M_D = \int_0^T \int_V \sigma \varepsilon^{ck} dV dt \qquad M_P = \int_0^T \int_V \sigma \varepsilon^{pl} dV dt \tag{5}$$

In the formula: T represents the duration of ground motion, V is the material volume, σ is the stress, ε^{ck} is the cracking strain, and ε^{pl} is the plastic strain.

The calculation results of earthquake damage in Section 4.1 are compared and analyzed from two dissipated energy indexes of damage (ALLDMD) and plastic (ALLPD). Under different cases, the overall damage dissipated energy and plastic dissipated energy values of the dam at the end of the earthquake action are shown in Fig.14. It can be seen from Fig.14(a) that under the action of three types of near-fault ground motions , the average overall damage dissipated energy of the dam is 12.72, 4.35 and 6.61 kN·m, respectively. Among them, the overall damage dissipated energy caused by the near-fault directivity pulse ground motion is the largest. Compared with the near-fault fling-step pulse and non-pulse, the dam overall damage dissipated energy increased by 192.41% and 92.44%, respectively. Fig.14(b) shows the overall plastic dissipated energy of the dam under different cases. Under the action of the three types of near-fault ground motions, the average values of the overall plastic dissipated energy of the dam is 61.43, 18.19 and 28.38 kN·m, respectively. Similar to the overall damage dissipated energy of the dam, the overall plastic dissipated energy caused by the near-fault directivity pulse ground motion is the largest, Compared with the near-fault fling-step pulse and the non-pulse, the dam overall plastic dissipated energy index increases respectively 237.71% and 116.46%.

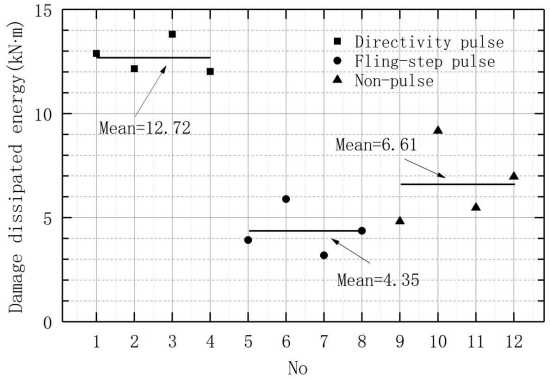

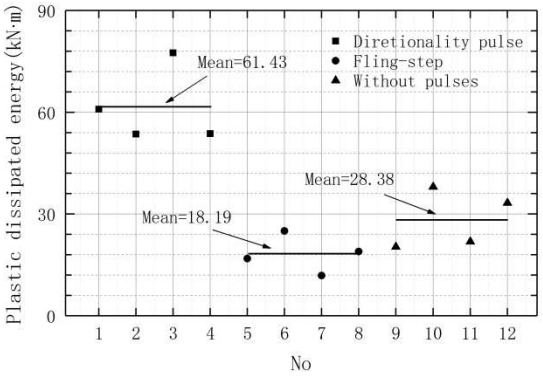

(a) Dam damage dissipated energy (b) Dam plastic dissipated energy

Fig.14 Overall dissipated energy of the dam

In order to deeply explore the impact of near-fault ground motions on the damage and failure of the concrete gravity dam, This paper compares the dissipated energy of the dam body and foundation respectively. It can be seen from Fig.15(a) that under the action of the near-fault directivity pulse ground motions, the damage dissipated energy values of the dam body and the dam foundation are relatively close, with an average ratio of about 0.98; The near-fault fling-step pulse ground motions cause no damage to the concrete material of the dam body; Under the action of near-fault non-pulse ground motions, the average ratio of the damage dissipated energy value of the dam body and foundation is about 0.25; Similarly, see Fig.15(b), under the action of the near-fault directivity pulse ground motions, the average ratio of the plastic dissipated energy of the dam body and foundation is about 1.01; Under the action of near-fault non-pulse ground motions, the average ratio of plastic dissipated energy between the dam body and foundation is about 0.24. Comparing the dissipated energy of the dam body and foundation under the three types of near-fault ground motions, it can be seen that under the action of near-fault directional pulsed ground motions, the dam body is more likely to be damaged and destroyed.

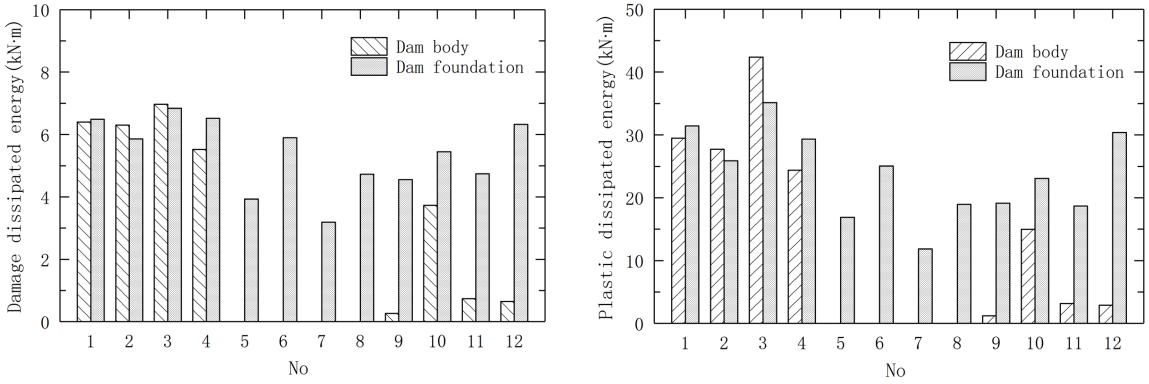

(a) Damage dissipated energy (b) Plastic dissipated energy

Fig.15 Energy dissipated of dam body and dam foundation

5.3. *Analysis of deformation characteristics of gravity dam structure*

The maximum horizontal displacement of the dam vertex obtained by nonlinear time history analysis is shown in Table 3. It can be seen from the table that under the action of directivity pulse ground motions, the average response of the horizontal displacement of the crest of the dam is the largest. The maximum average displacements in the upstream and downstream directions is 5.78 and 4.87 cm, respectively. The maximum average displacements in the upstream and downstream directions of the dam apex caused by non-pulse ground motions is 5.56 and 3.37 cm, respectively. The displacement response of the dam vertex caused by the fling-step pulse ground motion is 4.30 and 2.51 cm, respectively. From the perspective of the displacement amplitude of the dam vertex caused by ground motions, the relationship between the three working conditions is directivity pulse (10.66cm) > non-pulse (8.93cm) > fling-step pulse (6.81cm). Among them, the average amplitude of the dam vertex displacement caused by the directivity pulse ground motion is 1.19 times of the non-pulse and 1.57 times of the fling-step pulse.

Table 3 The horizontal displacement at crest of dam (cm)

Type	No	Horizontal displacement(max)	Average	Horizontal displacement(min)	Average	Displacement amplitude	Average
Directivity pulse	1	5.48	5.78	-4.35	-4.87	9.83	10.66
	2	5.74		-5.12		10.86	
	3	5.37		-5.70		11.07	
	4	6.52		-4.34		10.86	
Fling-step pulse	5	3.95	4.30	-2.75	-2.51	6.70	6.81
	6	4.57		-2.12		6.69	
	7	3.81		-3.04		6.85	
	8	4.86		-2.14		7.00	
Non-pulse	9	5.27	5.56	-2.50	-3.37	7.77	8.93

10	5.56	-4.05	9.61
11	5.41	-3.81	9.22
12	5.98	-3.12	9.10

In order to facilitate the comprehensive comparison of dam structural deformation caused by different types of near-fault ground motions, the method of expressing the dam deformation characteristics in reference (Liu et al. 2014) is given in the article. In this paper, three displacement angles ϕ_1, ϕ_1, and ϕ_3 are used to represent the residual deformation characteristics of the dam caused by near-fault ground motions.

$$\phi_1 = \frac{u_1 - u_2}{H} \qquad \phi_2 = \frac{u_3 - u_4}{h_1} \qquad \phi_3 = \frac{u_4 - u_5}{h_2} \tag{6}$$

In the formula: u_1 and u_2 respectively represent the residual horizontal displacement at the vertex and heel of the upstream dam face; u_3 and u_4 represent the residual horizontal displacement at the vertex of the downstream dam face and the downstream break slope respectively; u_5 represents the residual horizontal displacement at the dam toe. Among them, the relative displacement angle ϕ_1 reflects the overall deformation of the dam; ϕ_2 reflects the overall deformation of the dam head part; and ϕ_3 reflects the deformation of the lower structure of the dam.

Fig.16 shows the distribution of the mean value of each displacement angle under the action of three types of near-fault ground motions. Compared with the fling-step pulse and non-pulse ground motions, the directivity pulse ground motions can cause larger residual deformation of the dam structure, but it has little effect on the residual deformation of the lower part of the dam. Fig.17 shows the variation of the average horizontal residual displacement of the upstream face of the concrete gravity dam with respect to the dam heel under different cases. It can be seen that the impact of directivity pulse ground motions on the residual displacement of the upstream surface of the dam is significantly greater than that of fling-pulse and non-pulse. Under the action of near-fault directivity pulse and non-pulse ground motions , the horizontal displacement curve of the upstream surface of the dam has an inflection point in the middle. Under the action of the near-fault fling-step pulse ground motions, the average horizontal displacement of the upstream surface of the dam appears as a smooth straight line, and the average displacement increases with the increase of the dam height. This is because after the gravity dam is subjected to near-fault directivity pulse and non-pulse ground motions, the concrete at the downstream break slope has cracked damage, which causes the dam head to tilt in the upstream direction. However, under the action of near-fault sliding type ground motion, the dam concrete did not crack and damage.

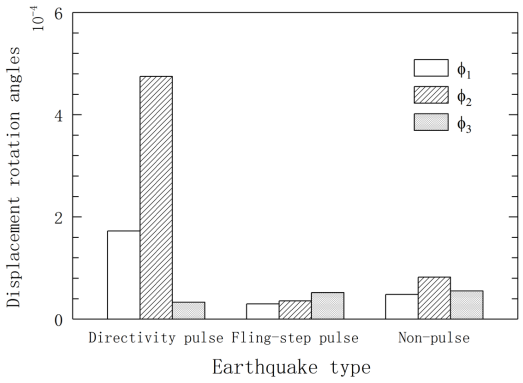

Fig.16 Characteristic value of each displacement angle

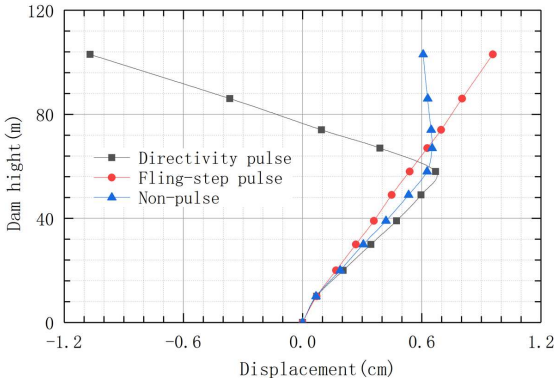

Fig.17 Displacement of the upstream of the dam along the river

6. Conclusion

This paper establishes a multi-coupling simulation model that can reasonably reflect the dynamic damage evolution process of dam concrete and dam foundation rock mass. Taking Koyna's measured seismic waves as input, the non-linear time history analysis of Koyna concrete gravity dam is carried out. The calculated results are more consistent with the actual seismic damage, which verifies the reliability of the overall damage model of the dam foundation used in this paper. To study the influence of near-fault ground motions on the overall dynamic damage of the concrete gravity dam, according to the characteristics of near-fault ground motions, this paper selects three types of near-fault ground motions with directivity pulse, fling-step pulse and non-pulse. Under the action of different types of near-fault earthquakes, the dynamic response of the concrete

gravity dam was analyzed from the three aspects of model damage zone, dissipated energy characteristics and dam displacement response. The research work has achieved the following understanding:

（1）Under the action of three types of near-fault ground motions, the dam foundation of the concrete gravity dam is damaged before the dam body. Among them, the directivity pulse ground motion has the greatest impact on the damage and failure of the concrete gravity dam, followed by the non-pulse ground motion, and the fling-step pulse ground motion is the smallest.

（2）From the perspective of dissipated energy characteristics. Under the action of near-fault directivity pulse-type ground motions, the plasticity dissipated energy and damage dissipated energy values of the dam body and the dam foundation are close. The dissipated energy caused by near-fault fling-step pulse and non-pulse ground motions is mainly concentrated in the dam foundation. Compared with the near-fault fling-step pulse and non-pulse ground motions, the damage and failure of the dam body caused by the directivity pulse ground motions should be paid more attention.

（3）From the perspective of the dam body deformation, directivity pulse ground motions can cause larger residual deformation of the dam overall structure and head part. However, the impact on the residual deformation of the lower part of the dam body is relatively small, this is because the directivity pulse ground motion cause larger damage and cracks on the downstream break slope, after the earthquake, the head of the dam tilted in the upstream direction. Under the action of the three types of near-fault ground motions, the average amplitude of the dam crest displacement caused by the directivity pulse ground motion is 1.2 times of the non-pulse and 1.57 times of the fling-step pulse.

In summary, compared with the fling-step pulse and non-pulse ground motions, directivity pulse ground motions have a significant impact on the nonlinear seismic response of concrete gravity dams. Therefore, it is necessary to consider the influence of near-fault directivity pulse ground motions when analyzing the seismic safety of concrete gravity dams. There has been the research result enunciation, more significant vertical ground motions in the near-fault area. If the vertical pulse ground motion is also considered, it will undoubtedly further increase the overall damage and failure of the the gravity dam. At present, there are few studies on the seismic response of gravity dam structures under the coupled action of pulse-type two-phase ground motions, and further research is still needed.

References

Akkse M, & Imek E (2010) Non-linear seismic response of concrete gravity dams to near-fault ground motions including dam-water-sediment-foundation interaction. Applied Mathematical Modelling, 34(11), 3685-3700. https://doi.org/10.1016/j.apm.2010.03.019

Ansari M I, & Agarwal P (2016) Damage index evaluation of concrete gravity dam based on hysteresis behavior and stiffness degradation under cyclic loading. International Journal of Structural Stability and Dynamics, 17(01), 1750009. https://doi.org/10.1142/s0219455417500092

Bayraktar A, T Türker, Akkse M, & Ate E (2010) The effect of reservoir length on seismic performance of gravity dams to near- and far-fault ground motions. Natural Hazards, 52(2), 257-275. https://doi.org/10.1007/s11069-009-9368-1

Bhagat S, Wijeyewickrema A C, & Subedi N (2018) Influence of near-fault ground motions with fling-step and forward-directivity characteristics on seismic response of base-isolated buildings. Journal of Earthquake Engineering, 1-20. https://doi.org/10.1080/13632469.2018.1520759

Bray J D, & Rodriguez-Marek A (2004) Characterization of forward-directivity ground motions in the near-fault region. Soil Dynamics & Earthquake Engineering. https://doi.org/10.1016/j.soildyn.2004.05.001

Chen H Q, Li D Y, & Guo S S (2014) Damage–rupture process of concrete dams under strong earthquakes. International Journal of Structural Stability & Dynamics, 14(07), 1450021. https://doi.org/10.1142/S0219455414500217

Durucan C, Ahin H, & Durucan A R (2021) A new ground motion intensity measure for short period reinforced concrete structures subjected to near-fault pulse-like ground motions. Mechanics Based Design of Structures and Machines(5), 1-16. https://doi.org/10.1080/15397734.2021.1886114

Eftekhari N, Sayyadpour H, & Kowsari M (2020) A near-fault probabilistic seismic hazard assessment for yasouj, located in the kazerun fault system, southwest iran. Natural Hazards(3). https://doi.org/10.1007/s11069-020-04384-z

Gao Z, Zhao M, Du X, & Zhong Z (2021) A generalized response spectrum method for seismic response analysis of underground structure combined with viscous-spring artificial boundary. Soil Dynamics and Earthquake Engineering, 140, 106451. https://doi.org/10.1016/j.soildyn.2020.106451

Gorai S, & Maity D (2021) Numerical investigation on seismic behaviour of aged concrete gravity dams to near source and far source ground motions. Natural Hazards. https://doi.org/10.1007/s11069-020-04344-7

Guo S, Liang H, Wu S, Xiong K, & Zhang A (2020) Seismic damage investigation of arch dams under different water levels based on massively parallel computation. Soil Dynamics and Earthquake Engineering, 129, 105917-. https://doi.org/10.1016/j.soildyn.2019.105917

Hadiani M (2013) Seismic response of embankment dams under near-fault and far-field ground motion excitation. Engineering Geology. https://doi.org/10.1016/j.enggeo.2013.02.008

Hebbouche A, Bensaibi M, & Mroueh H (2013) Seismic risk analysis of concrete gravity dams under near-fault ground motions. Applied Mechanics and Materials, 256-259, 2240-2243. https://doi.org/10.4028/www.scientific.net/AMM.256-259.2240

Huang J (2015) Earthquake damage analysis of concrete gravity dams: modeling and behavior under near-fault seismic excitations. Journal of Earthquake Engineering, 19(7-8), 1037-1085. https://doi.org/10.1080/13632469.2015.1027019

Kao H, Liu Y H, Liang W T, & Chen W P (2002) Source parameters of regional earthquakes in taiwan: 1999-2000 including the ch-chi earthquake sequence. Terrestrial Atmospheric and Oceanic Sciences, 13(3). https://doi.org/10.3319/TAO.2002.13.3.279(CCE)

Kate, Huihsuan, & Chen (2011) Observations of changes in waveform character induced by the 1999 mw7.6 chi-chi earthquake. Geophysical Research Letters. https://doi.org/10.1029/2011GL049841

Lee J, & Fenves G L (1998) A plastic-damage concrete model for earthquake analysis of dams. Earthquake Engineering & Structural Dynamics, 27(9). https://doi.org/10.1002/(SICI)1096-9845(199809)27:93.0.CO;2-5

Li S, Liu J, Yang Z, Bao X & Asheghabadi M S (2020) Multiscale method for seismic response of near-source sites. Advances in Civil Engineering, 2020(2), 8183272. https://doi.org/10.1155/2020/8183272

Li Z, Wu Z, J Chen, Lu X, & Chen C (2021) Effect of correlated random fields on nonlinear dynamic responses of gravity dam. Natural Hazards, 106(3). https://doi.org/10.1007/s11069-020-04451-5

Liu Z J, Zeng B, Zhou Y H, & Tian B (2014) Probabilistic model of ground motion processes and seismic dynamic reliability analysis of the gravity dam. Journal of Hydraulic Engineering, 45(9), 1066-1074. https://doi.org/10.13243/j.cnki.slxb.2014.09.007

Sadeghi M H, & Moradloo J (2020) Seismic analysis of damaged concrete gravity dams subjected to mainshock-aftershock sequences. European Journal of Environmental and Civil Engineering(4), 1-22. https://doi.org/10.1080/19648189.2020.1763475

Suarez-Villa L, & Walrod, W (2010) Losses from the northridge earthquake: disruption to high-technology industries in the los angeles basin. Disasters, 23(1), 19-44. https://doi.org/10.1111/1467-7717.00103

Tong M, Rzhevsky V, Dai J, Lee G C, Qi J, & Qi X (2007) Near-fault ground motions with prominent acceleration pulses: pulse characteristics and ductility demand. Earthquake Engineering & Engineering Vibration, 6(3), 215-223. https://doi.org/10.1007/s11803-007-0762-y

Wang G, Zhang S, Chao W, & Mao Y (2014) Seismic performance evaluation of dam-reservoir-foundation systems to near-fault ground motions. Natural Hazards, 72(2), 651-674. https://doi.org/10.1007/s11069-013-1028-9

Wang G, Zhang S, Zhou C, & Lu W (2014) Correlation between strong motion durations and damage measures of concrete gravity dams. Soil Dynamics and Earthquake Engineering, 69, 148-162. https://doi.org/10.1016/j.soildyn.2014.11.001

Yang F, Wang G, & Ding Y (2019) Damage demands evaluation of reinforced concrete frame structure subjected to near-fault seismic sequences. Natural Hazards, 97(1). https://doi.org/10.1007/s11069-019-03678-1

Yazdani Y, Alembagheri, & M (2017) Nonlinear seismic response of a gravity dam under near-fault ground motions and equivalent pulses. Soil dynamics and earthquake engineering. https://doi.org/10.1016/j.soildyn.2016.11.003

Yujia Guo, Kazuki, Koketsu, Taichi, & Ohno (2013) Analysis of the rupture process of the 1995 kobe earthquake using a 3d velocity structure. Earth Planets & Space. https://doi.org/10.5047/eps.2013.07.006

Zhai Y, Bi Z, Tang Y, et al (2020) Study on damage and failure of gravity dam under main aftershock sequence based on NGA Model. Journal of Hydraulic Engineering, 51(02):152-157+168. https://doi.org/10.13243/j.cnki.slxb.20190749

Zhang L, Zhai Y, Cui B, Tang Y, & Bi Z (2021) A novel method for constructing main-aftershock sequences and its application in the global damage accumulation effects analysis of gravity dams. Shock and Vibration, (3), 1-12. https://doi.org/10.1155/2021/9356540

Zhang S, & Wang G (2013) Effects of near-fault and far-fault ground motions on nonlinear dynamic response and seismic damage of concrete gravity dams. Soil Dynamics & Earthquake Engineering, 53, 217-229. https://doi.org/10.1016/j.soildyn.2013.07.014

Zhang S, Wang G, Pang B, & Du C (2013) The effects of strong motion duration on the dynamic response and accumulated damage of concrete gravity dams. Soil Dynamics and Earthquake Engineering, 45(1), 112-124. https://doi.org/10.1016/j.soildyn.2012.11.011

Zou D, Han H, Liu J, Yang D, & Kong X (2017) Seismic failure analysis for a high concrete face rockfill dam subjected to near-fault pulse-like ground motions. Soil Dynamics and Earthquake Engineering, 98, 235-243. https://doi.org/10.1016/j.soildyn.2017.03.031

Funding

This research was financially supported by Nation key Research and Development Plan of Ministry of science and technology of the People 's Republic of China(2017YFC0404903), the National Natural Science Foundation of China(51709090) and the Natural Science Foundation of Jiangsu Province (BK20170884).

Conflicts of Interest

The authors declare that there is no conflict of interest regarding the publication of this paper.

Availability of data and material

The data and material used to support the findings of this study are included within the article or are cited at relevant places within the text as references.

Author Contributions

Yafei Zhai and Liaojun Zhang carried out the article topic selection, definition of intellectual content and model analysis. Hanyun Zhang provided assistance for data analysis and literature, in addition, Liaojun Zhang and Hanyun Zhang provided financial support. Tianxiao Ma and Binghui Cui performed Manuscript editing and manuscript review. All authors have read and agreed to the published version of the manuscript.

Ethics approval

Approved.

Consent to participate

Yes.

Consent for publication

Yes.

Figures

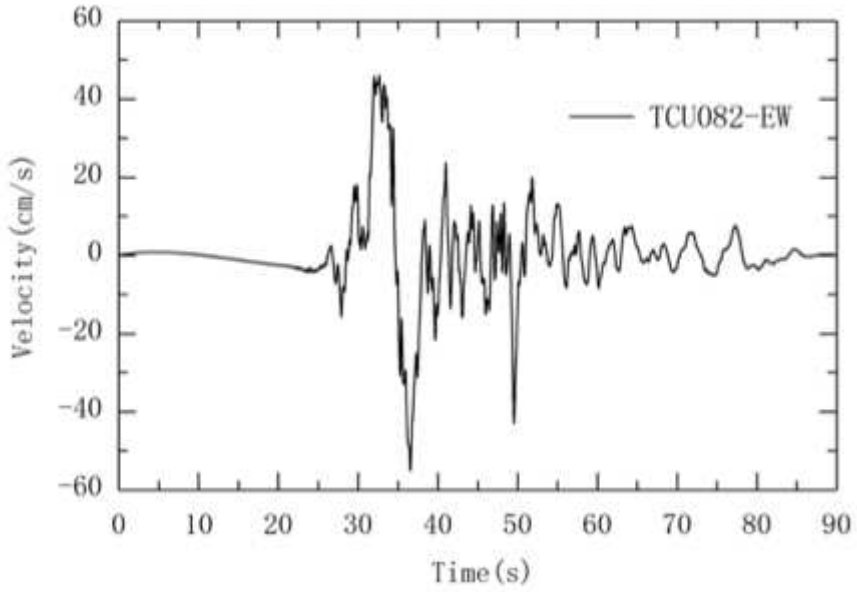

Figure 1

Velocity time history of directivity pulse ground motion

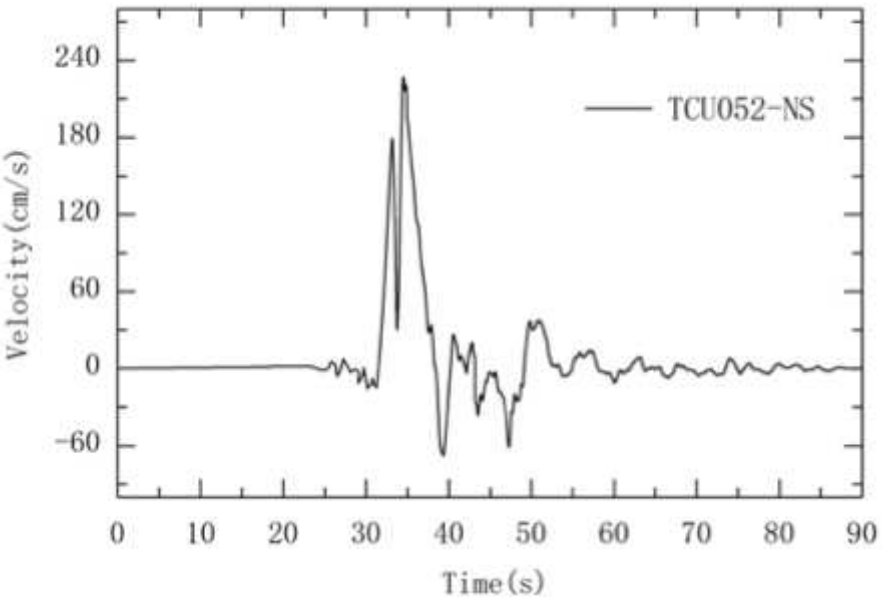

Figure 2

Velocity time history of fling-step pulse ground motion

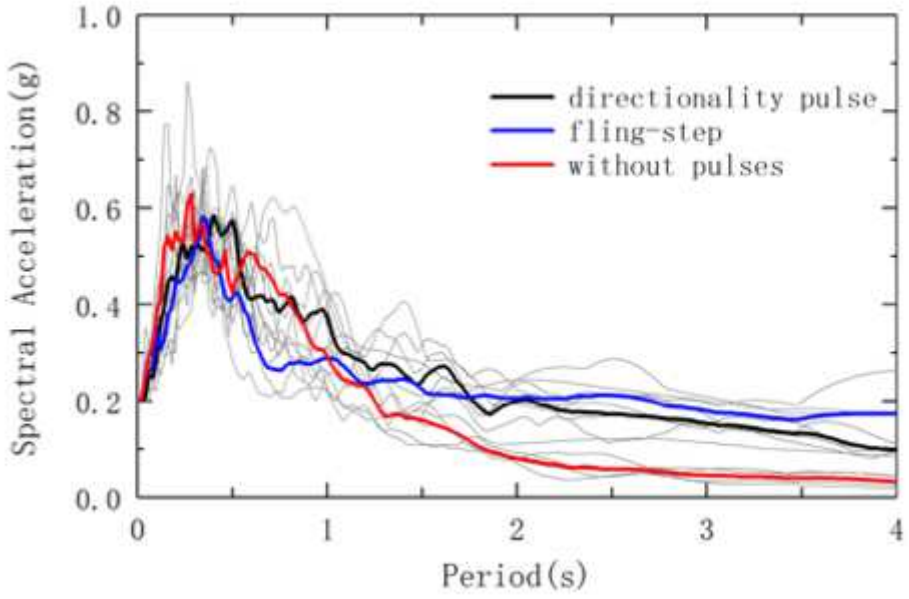

Figure 3

Acceleration response spectrum

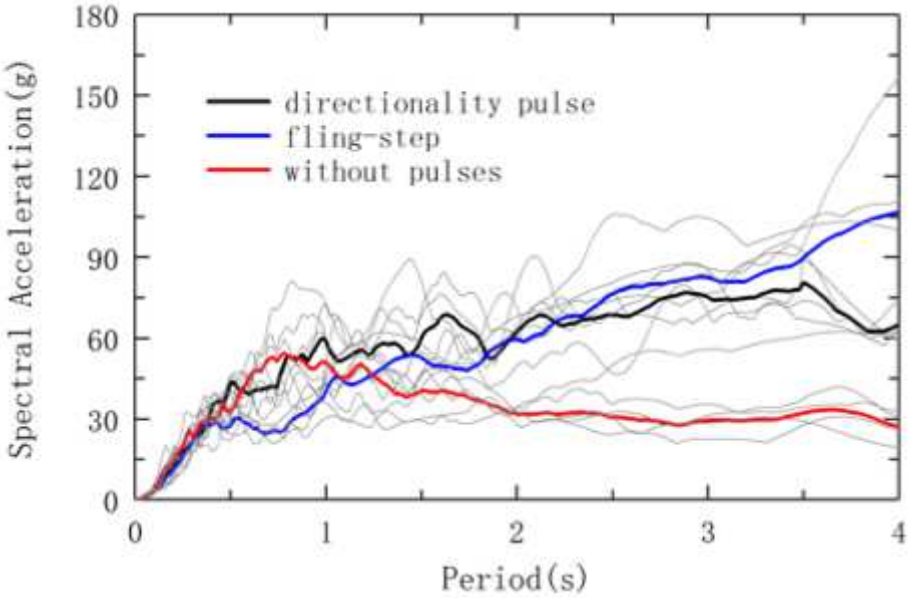

Figure 4

Speed response spectrum

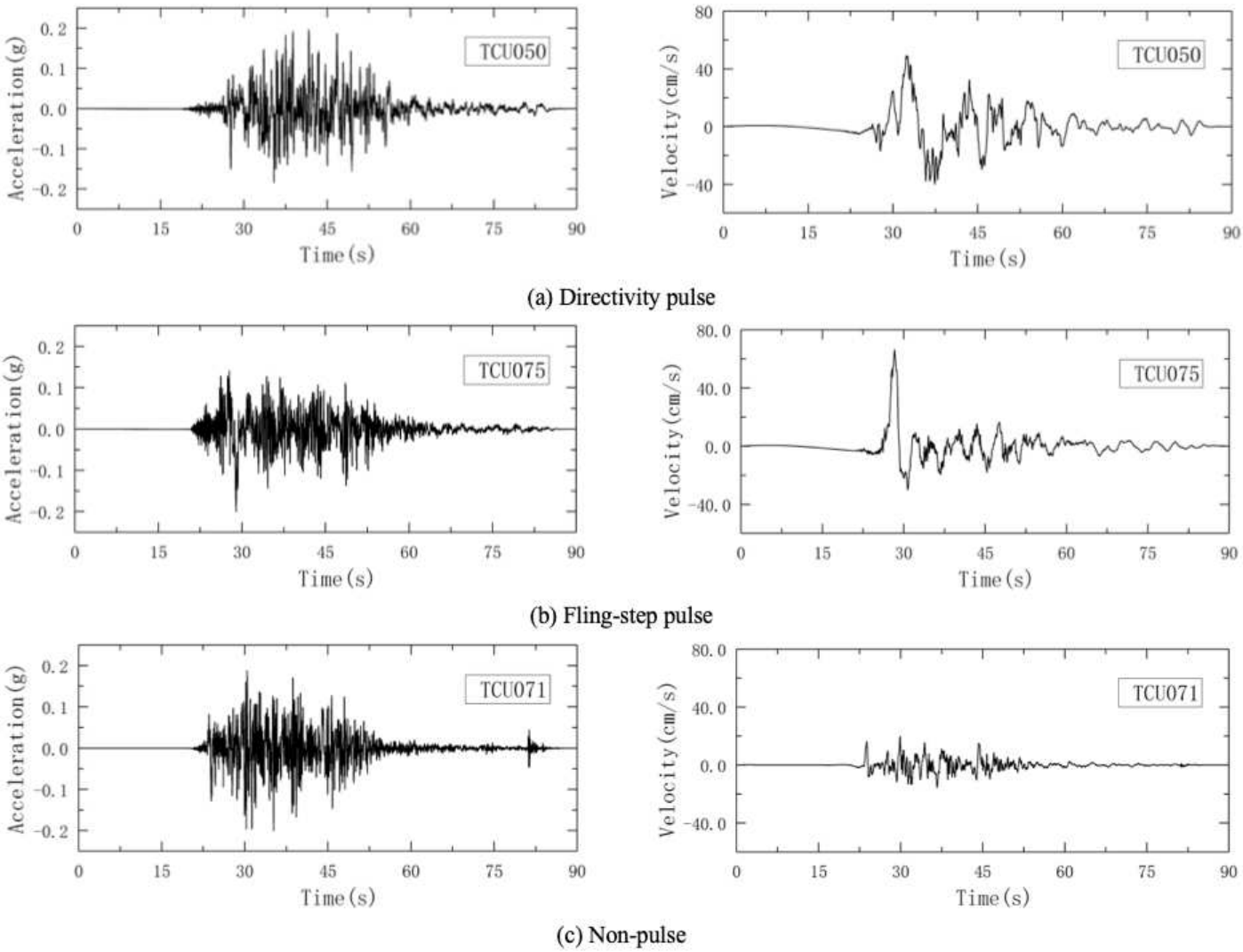

Figure 5

Curves of acceleration and velocity of the typical near-fault ground motion

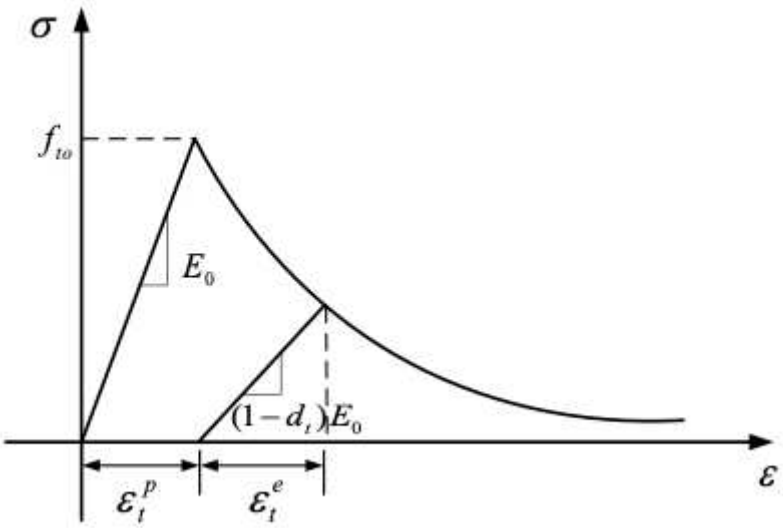

Figure 6

Schematic diagram of concrete uniaxial tensile damage

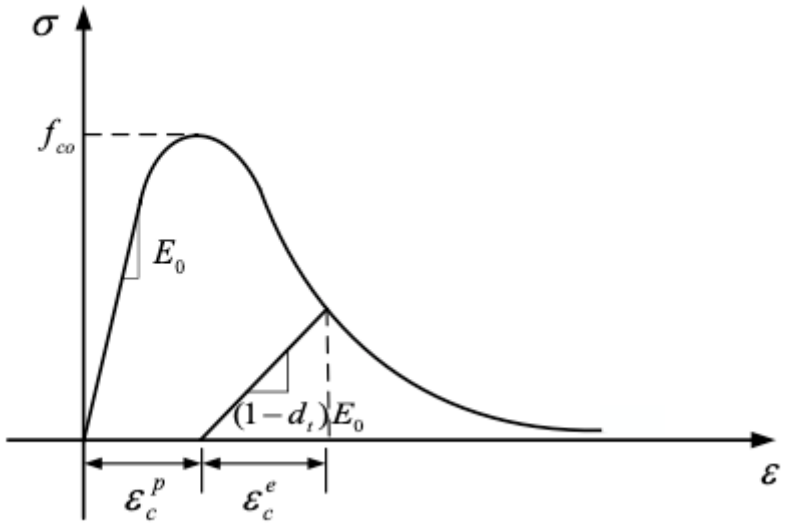

Figure 7

Schematic diagram of concrete uniaxial compression damage

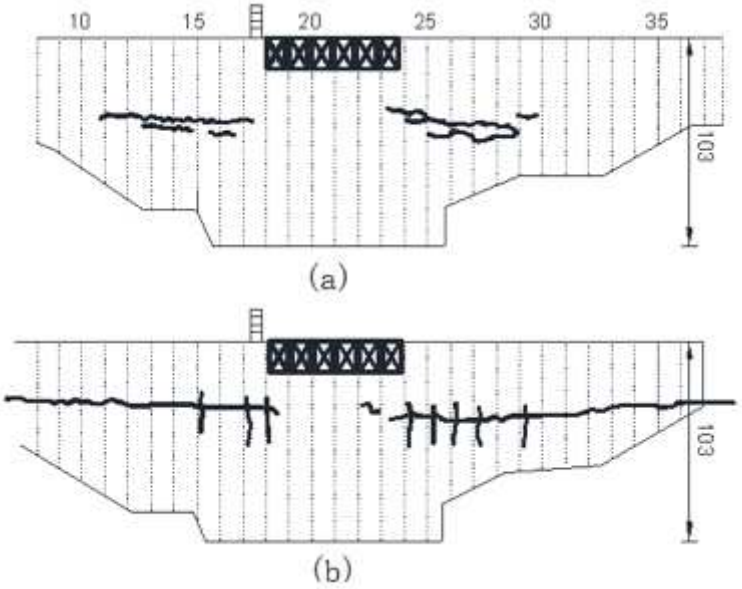

Figure 8

Earthquake damage to Koyna Dam (a: upstream view, b: downstream view)

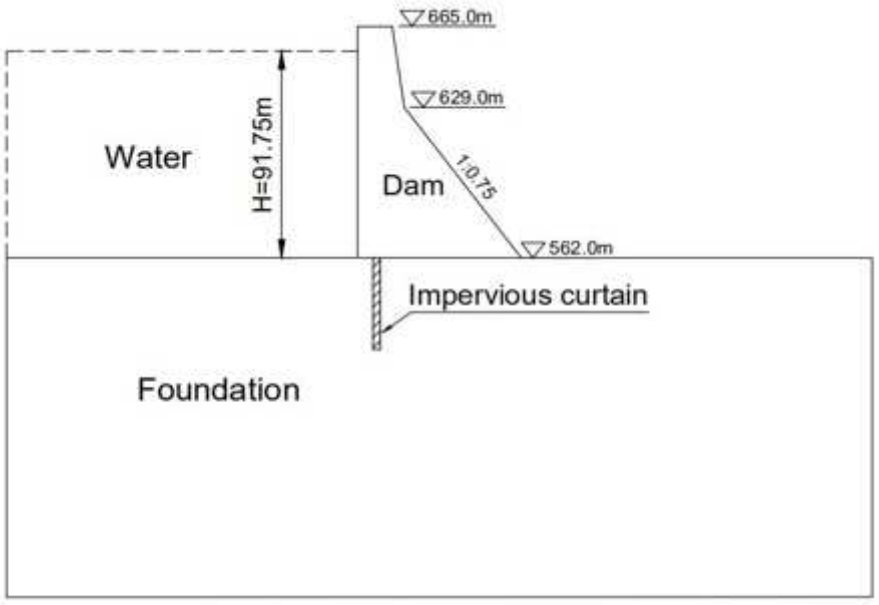

Figure 9

Dam body-reservoir water-foundation model

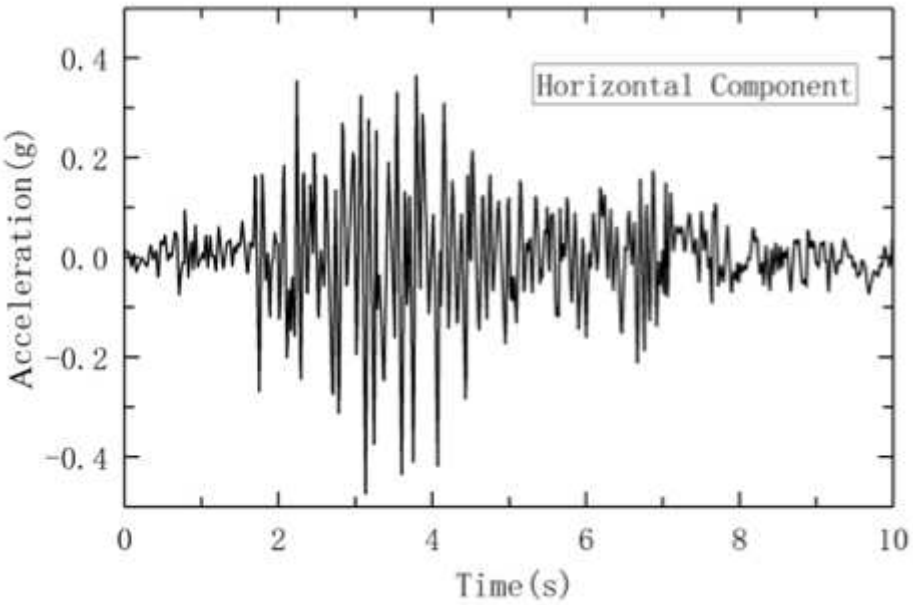

Figure 10

Acceleration time history curve of horizontal seismic wave

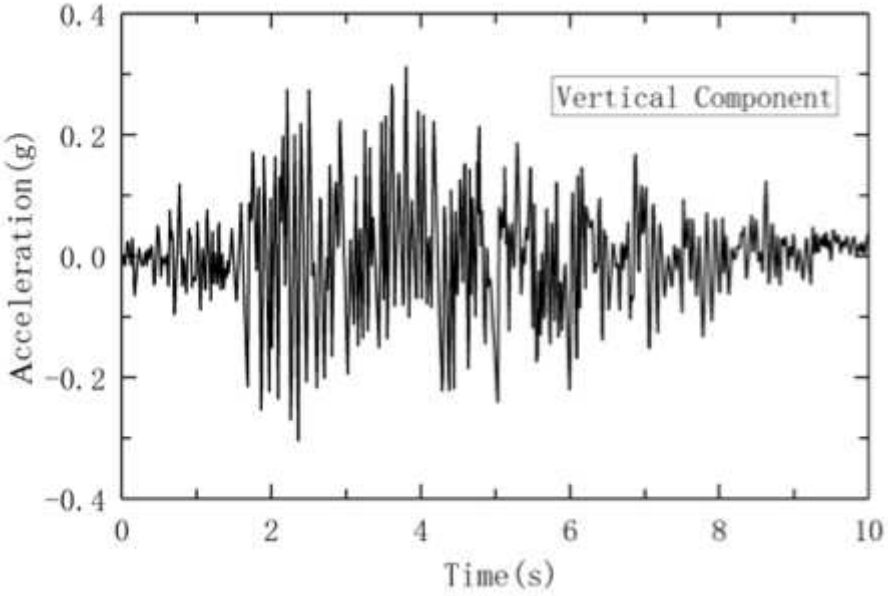

Figure 11

Acceleration time history curve of vertical seismic wave

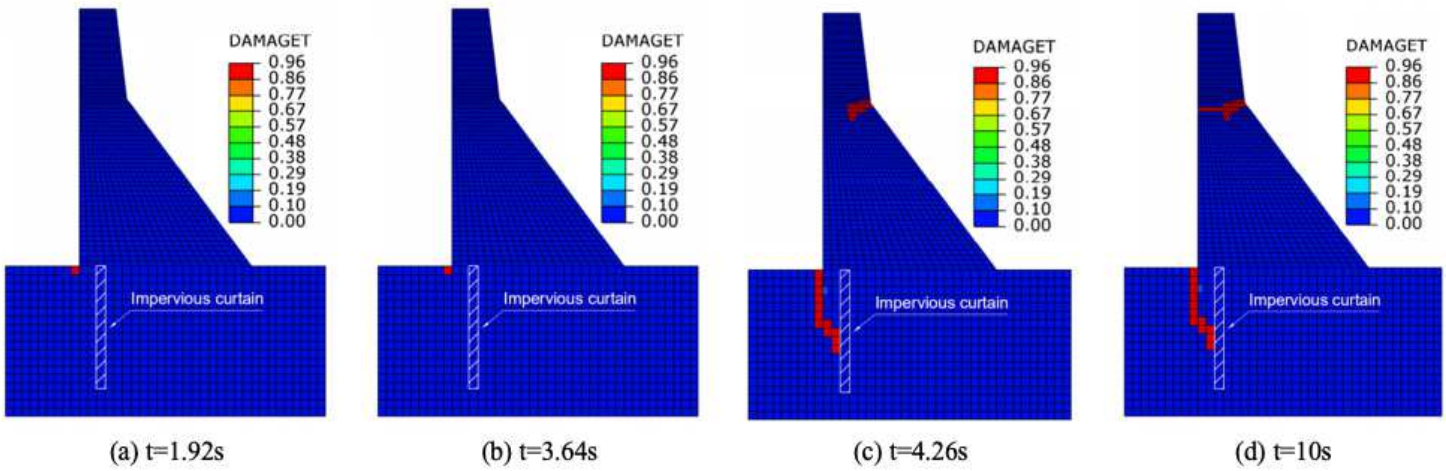

Figure 12

Damage zone of gravity dam at different times

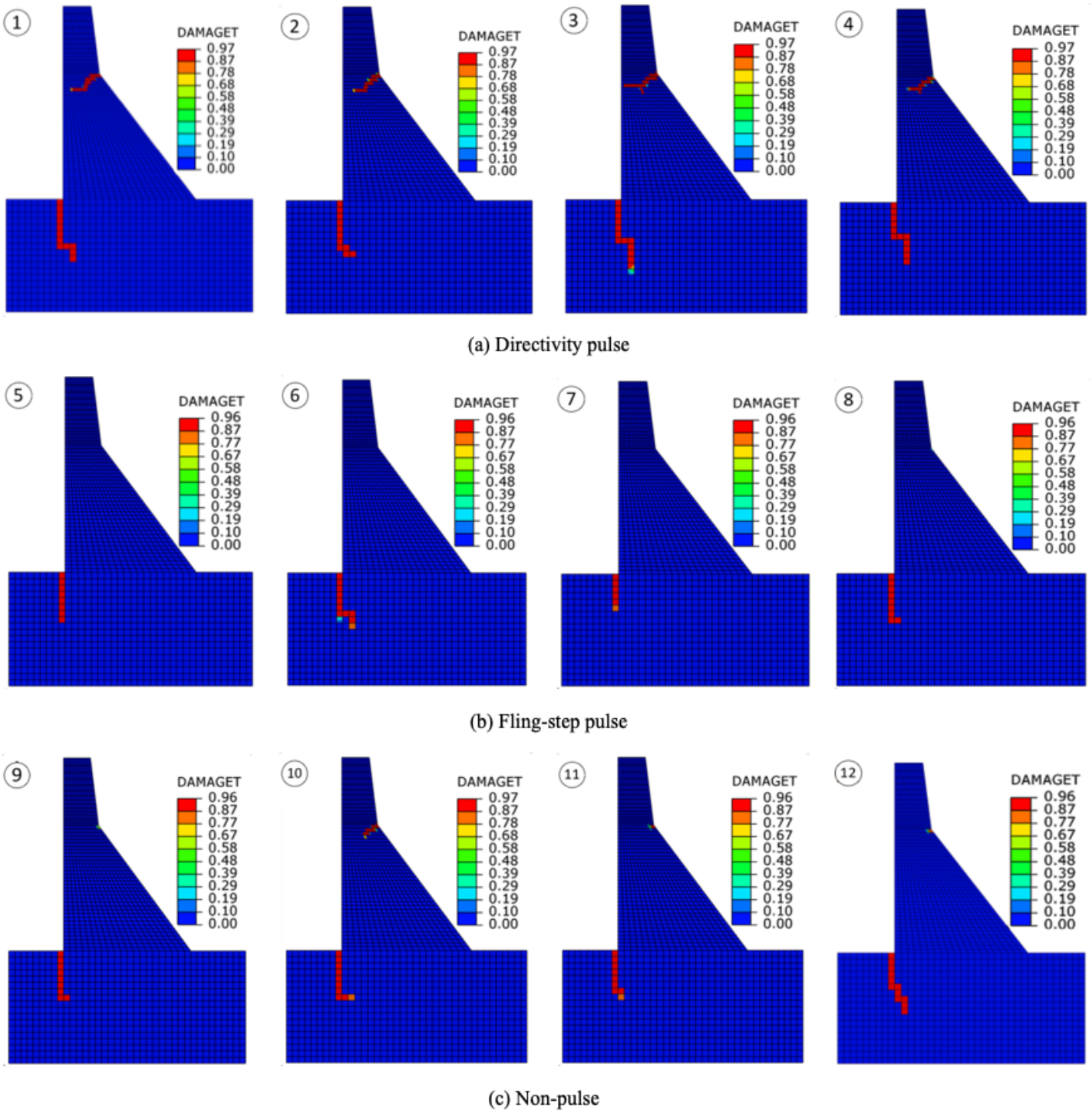

Figure 13

Dam damage zone of near-fault ground motions (1,2...represent the seismic wave number)

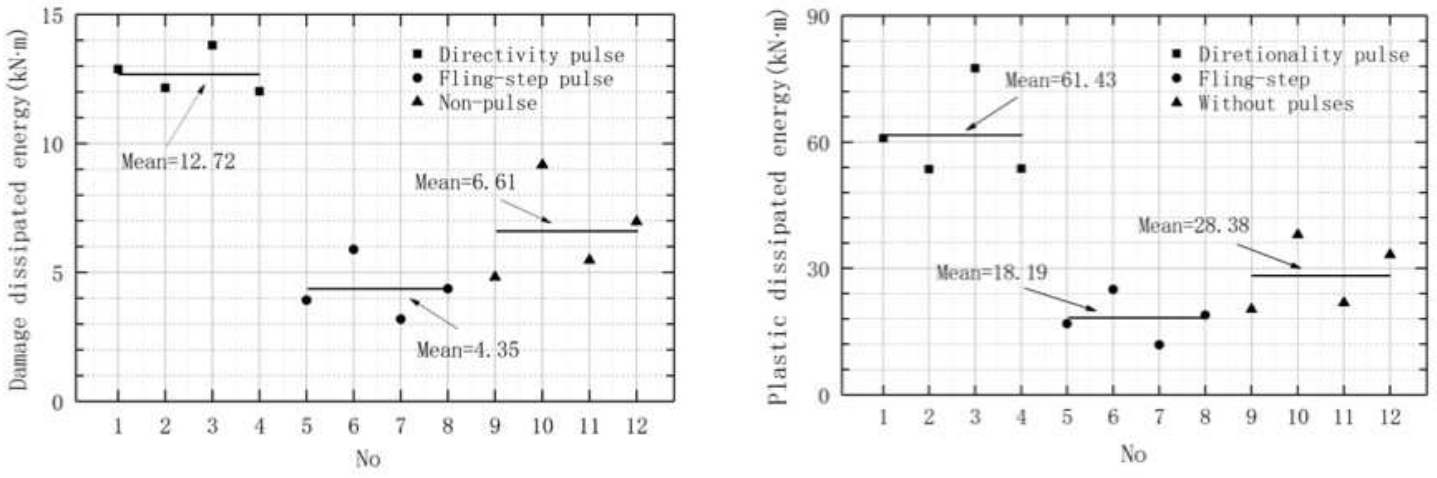

(a) Dam damage dissipated energy

(b) Dam plastic dissipated energy

Figure 14

(a) Dam damage dissipated energy (b) Dam plastic dissipated energy

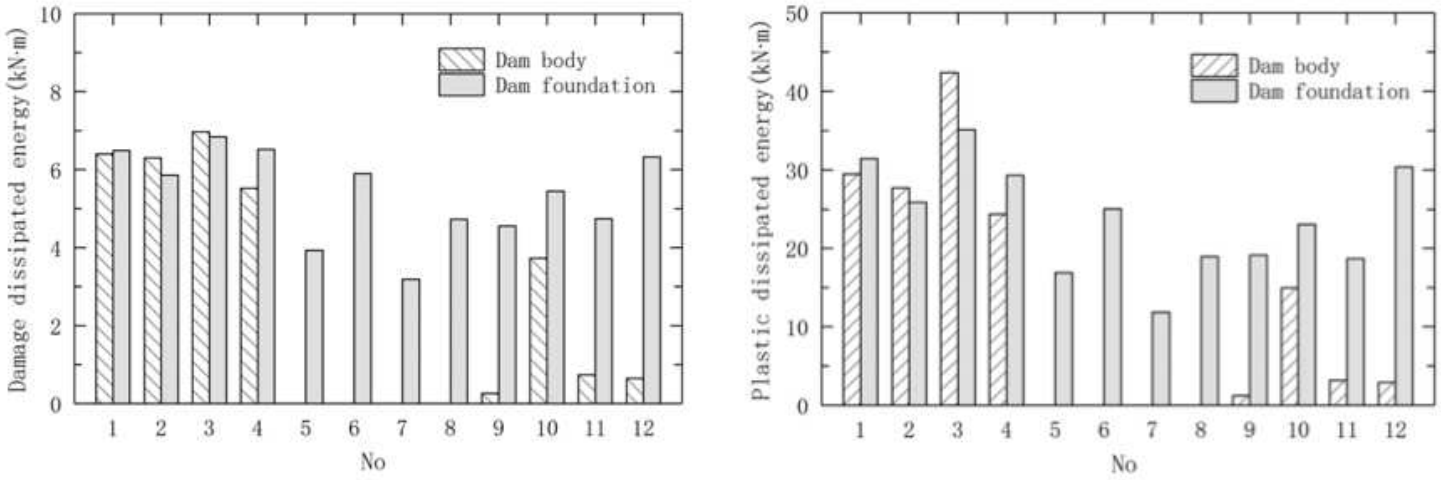

(a) Damage dissipated energy

(b) Plastic dissipated energy

Figure 15

(a) Damage dissipated energy (b) Plastic dissipated energy

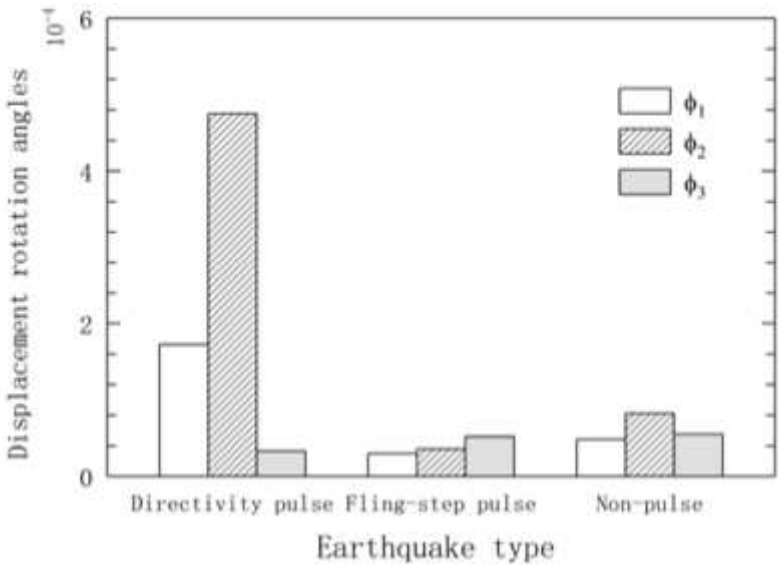

Figure 16

Characteristic value of each displacement angle

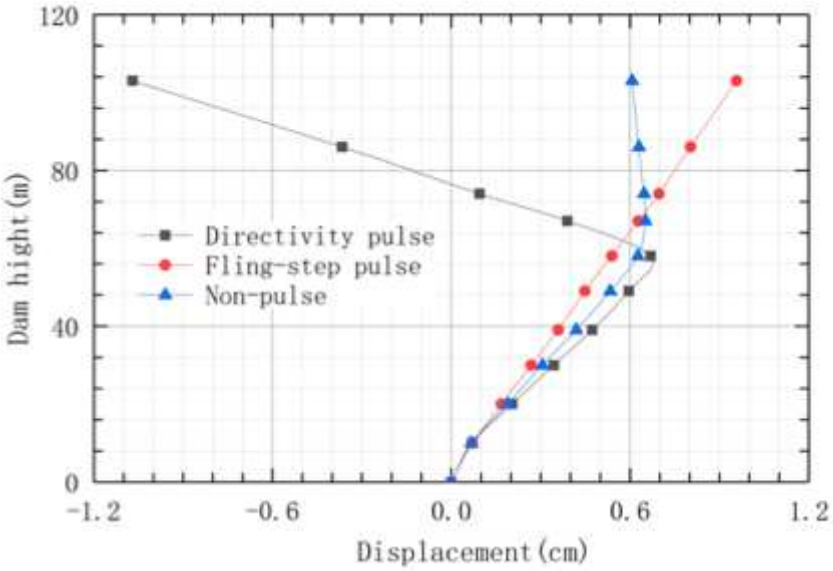

Figure 17

Displacement of the upstream of the dam along the river